

The Ubiquity of Supermassive Black Holes in the Hubble Sequence

Francine R. Marleau, Dominic Clancy and Matteo Bianconi

Institute of Astro and Particle Physics, University of Innsbruck, 6020 Innsbruck, Austria

Accepted 8 August 2013

ABSTRACT

We present the results of a study of a statistically significant sample of galaxies which clearly demonstrate that supermassive black holes are generically present in all morphological types. Our analysis is based on the quantitative morphological classification of 1.12 million galaxies in the SDSS DR7 and on the detection of black hole activity via two different methods, the first one based on their X-ray/radio emission and the second one based on their mid-infrared colors. The results of the first analysis confirm the correlation between black hole and total stellar mass for 8 galaxies and includes one galaxy classified as bulgeless. The results of our second analysis, consisting of 15,991 galaxies, show that galaxies hosting a supermassive black hole follow the same morphological distribution as the general population of galaxies in the same redshift range. In particular, the fraction of bulgeless galaxies, 1,450 galaxies or 9 percent, is found to be the same as in the general population. We also present the correlation between black hole and total stellar mass for 6,247 of these galaxies. Importantly, whereas previous studies were limited to primarily bulge-dominated systems, our study confirms this relationship to all morphological types, in particular, to 530 bulgeless galaxies. Our results indicate that the true correlation that exists for supermassive black holes and their host galaxies is between the black hole mass and the total stellar mass of the galaxy and hence, we conclude that the previous assumption that the black hole mass is correlated with the bulge mass is only approximately correct.

Key words: galaxies: general — galaxies: Seyfert — galaxies: active — galaxies: spiral — galaxies: bulges — galaxies: evolution — infrared: galaxies

1 INTRODUCTION

According to the standard picture, the structure we observe today in our Universe formed as a consequence of the growth of fluctuations in the primordial dark matter distribution which gravitationally attracted gaseous baryonic matter that later settled into disk galaxies (e.g. [White & Rees 1978](#); [White & Frenk 1991](#)). Galaxy mergers within halos subsequently transformed disks into bulges and the gas fell to the center, triggering starbursts and feeding the rapid growth of black holes (BH). These in turn responded by feeding energy back to the surrounding gas (e.g. [Sanders et al. 1988](#); [Hopkins et al. 2008](#)). This picture of structure formation is based on observational work which, over the past few decades, indicates that most -if not all- *massive* galaxies with a spheroidal component have a supermassive black hole (SMBH) at their center (e.g. [Kormendy & Richstone 1995](#); [Magorrian et al. 1998](#)). In addition, estimates of the BH masses of these giant galaxies have been found to tightly correlate with the spheroid/host luminosity (or stellar mass) and also with the stellar velocity dispersion within the

host bulges (e.g. [Gebhardt et al. 2000](#); [Ferrarese & Merritt 2000](#)).

However, there is growing evidence that SMBH not only exist at the centers of massive galaxies with a central bulge, but also at the centers of galaxies with pseudo-bulges and that these systems also exhibit a correlation between black hole mass and total stellar mass ([Jiang et al. 2011](#); [Simmons et al. 2013](#)). This supports the alternative view that SMBH growth might be due to minor mergers and/or secular processes (e.g. [Greene et al. 2010](#); [Simmons et al. 2013](#)). Although, as pointed out by [Okamoto \(2012\)](#), the main channel of pseudo-bulge formation may in fact not be secular disk evolution but rather rapid gas supply at high-redshift.

Given the uncertainties concerning the current understanding of the formation of bulges and pseudo-bulges in galaxies, the problem of identifying the main process at play in the formation of SMBH at the centers of galaxies with a spheroidal component remains a difficult challenge at present. On the other hand, the recent discovery of a SMBH at the center of Henize 2-10 ([Reines et al. 2011](#)), a dwarf

starburst galaxy lacking any substantial spheroidal component, suggests that a merger is not essential to making a SMBH and that BH growth may after all require substantial and ongoing secular processes, at least in these galaxies. Indeed, recent theoretical developments on the formation of the first massive BH show that they may form out of gas-dynamical instability at low metallicity (e.g. [Volonteri 2012](#)). Moreover, if SMBH are also generic to bulgeless galaxies and dwarf galaxies, as indeed the current work will present evidence to demonstrate they are, these galaxy types may offer the best probe of SMBH formation and evolution in the local Universe. In this regard, a SMBH hosted by a bulgeless galaxy and/or dwarf galaxy is more likely “pristine”, as it is unlikely that it has experienced mergers and dynamical interactions but has rather undergone a quieter evolution. Moreover, pure-disk galaxies are far from rare: locally, only four of the nineteen giant galaxies are ellipticals or have classical bulges ([Kormendy et al. 2010](#)). While in the Sloan Digital Sky Survey (SDSS; [York et al. 2000](#)), based on the quantitative morphological analysis of 1.12 million galaxies in the Data Release Seven (DR7; [Abazajian et al. 2009](#)), the fraction of galaxies with an optical Sérsic profile index $n_g < 1.5$ and bulge fraction $B/T < 0.1$, i.e. nearly bulgeless, is $\sim 14\%$ ([Simard et al. 2011](#), hereafter [S11](#)). However, despite the large fraction of bulgeless galaxies and their clear importance in challenging our current understanding of galaxy formation and evolution, a systematic survey of SMBHs in bulgeless galaxies has never been undertaken, though this is in part due to the lack of a well-defined sample. In this paper, we attempt to rectify this situation and substantially extend the status of the present knowledge of SMBH and their host galaxies by presenting the first systematic survey of SMBHs in galaxies of all morphological types, i.e. including those classified as bulgeless galaxies, based on the quantitative morphological analysis of 1.12 million galaxies in the SDSS DR7 ([S11](#)).

In this work we report the results of two separate studies which explore the nature of SMBH and their host galaxies, the first based on an X-ray/radio selected sample and the second on an infrared selected sample. The structure of our paper is as follows. In [Section 2](#), we describe the method that we used to select our sample of morphologically classified galaxies. In [Section 3](#), we present the selection and analysis of our X-ray/radio selected sample of active SMBH, while in [Section 4](#), we present the selection and analysis of our infrared selected sample of active SMBH. In [Section 5](#), we summarize our results. Considered together, we believe these two studies are complementary in nature, in that while our first analysis of an X-ray selected sample provides a well-tested and robust estimate of black hole mass but with a small statistic, our second analysis of an infrared selected sample provides estimates on the black hole mass, parametrised by their accretion efficiency, but with a large statistic.

2 QUANTITATIVE MORPHOLOGICAL PARAMETERS

As the foundation of all our work we used the quantitative morphological classification of [S11](#) to extract structural parameters for 1.12 million galaxies. In this work, the sources that were fitted were selected from the Legacy area with

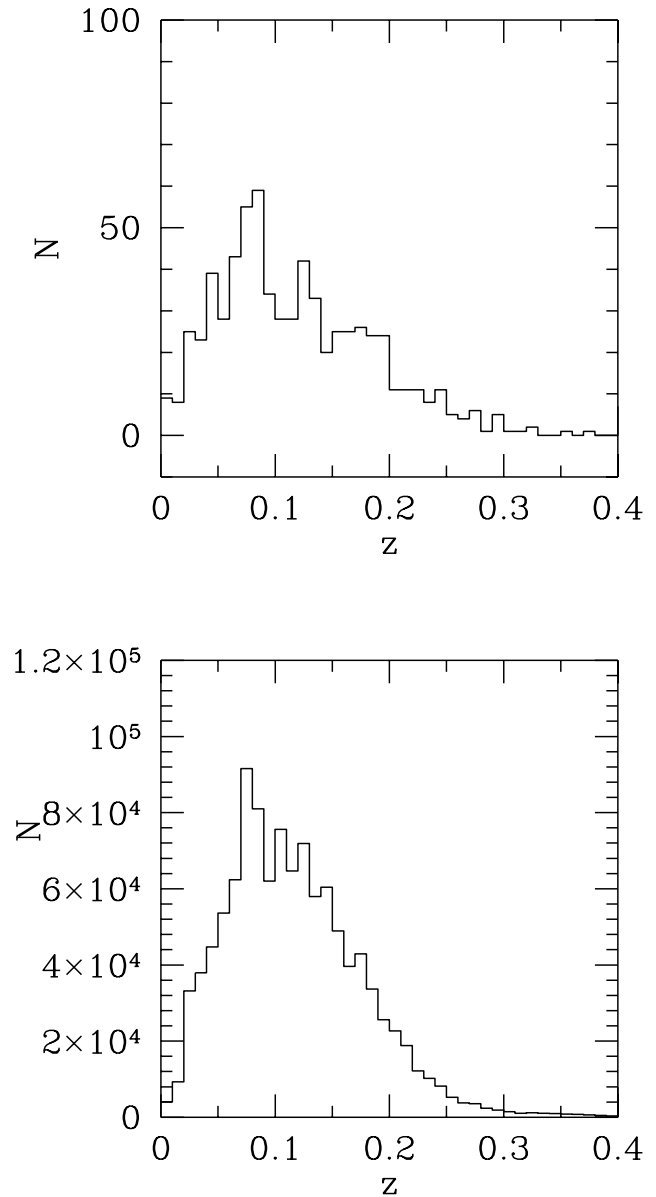


Figure 1. *Top:* Redshift distribution of the 688 galaxies in the CSC-SDSS catalog with structural parameters. *Bottom:* Redshift distribution of the SDSS DR7 galaxies in the [S11](#) morphological catalog.

$14.0 \leq m_r \leq 18.0$, where m_r is the r -band Petrosian magnitude corrected for Galactic extinction according to the extinction values given in the SDSS database, and morphological type Type = 3, i.e. sources classified as galaxies. In addition to these two criteria, the sum of the flags DEBLENDED_AS_PSF and SATURATED were required to be zero to eliminate objects that were found to be unresolved children of their parents as well as saturated objects. The total number of objects in the [S11](#) catalog is 1,123,718.

Galaxy structural parameters obtained by [S11](#) were measured from bulge + disk decompositions performed

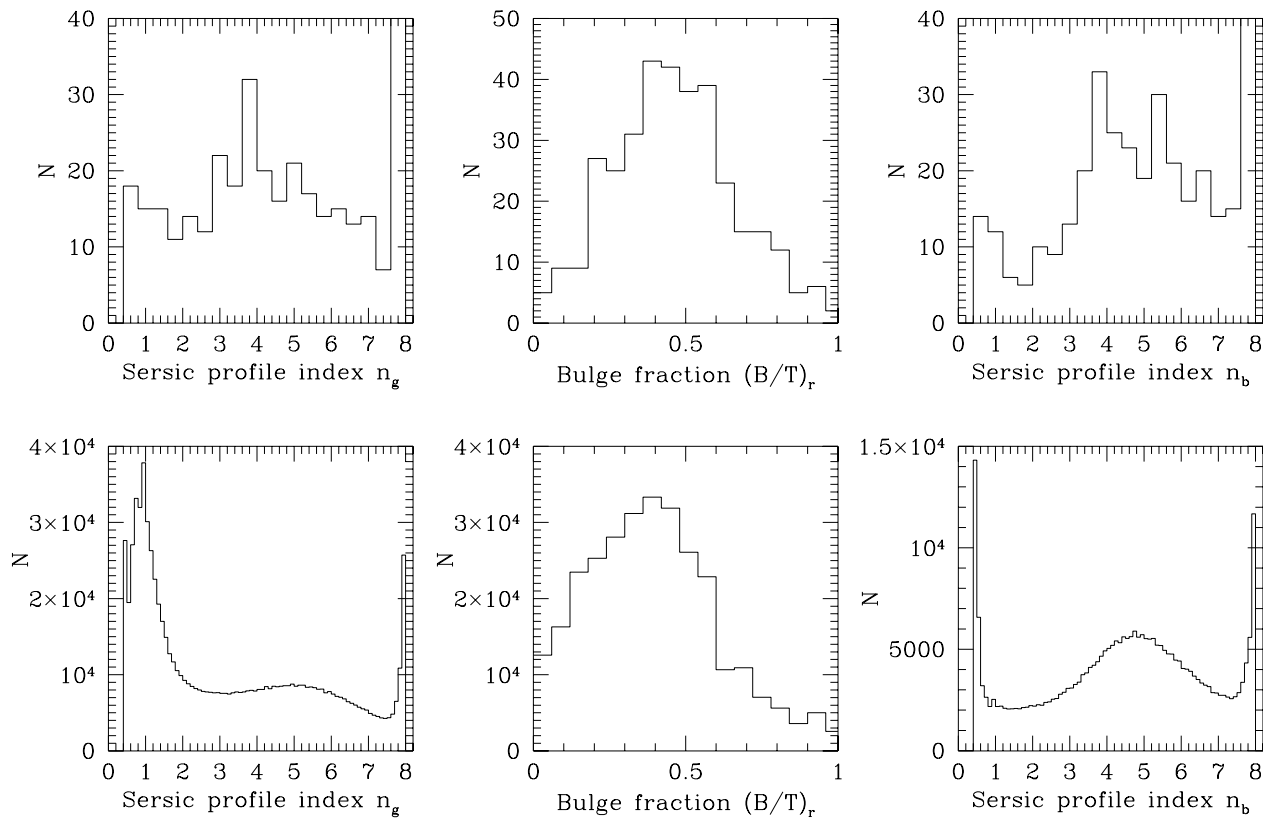


Figure 2. *Top row:* Distribution of the Sérsic index n_g (left), the bulge fraction $(B/T)_r$ (middle) and the bulge Sérsic index n_b (right) of the galaxies in the CSC-SDSS catalog with structural parameters. *Bottom row:* Distribution of the Sérsic profile index n_g (left), the bulge fraction $(B/T)_r$ (middle) and the bulge Sérsic index n_b (right) of the SDSS DR7 galaxies in the S11 morphological catalog.

using version 3.2 of the GIM2D software package (Simard et al. 2002). In addition to the canonical de Vaucouleurs bulge (Sérsic index $n_b = 4$) + exponential disk fitting model (S11, Table 1), two other fitting models were used. The first additional model was a free n_b bulge + disk model, with n_b allowed to vary from 0.5 to 8 (S11, Table 2), and the second one was a single component pure Sérsic model, with n_g also allowed to vary from 0.5 to 8 (S11, Table 3). The appropriate model was selected using the F-test probability P_{pS} and the uncertainties associated with the best fit parameters were estimated from the 99% confidence limits (Table 1-3, S11; Marleau & Simard 1998).

In order to classify a galaxy as bulgeless, we required an optical Sérsic profile index $n_g < 1.5$ and a bulge fraction $B/T < 0.1$. For the whole S11 catalog, this yielded a list of 88,594 galaxies, corresponding to about 14% of the total sample. As shown by Kelvin (2013), the ability of the quantitative code to recover bulges is limited by the resolution of the images, in this case 1.2 arcsec. For a typical bulge of size 3 kpc (S11), quantitative methods can recover bulges in the SDSS images to a redshift of about 0.06. Assuming a size distribution that is Gaussian, we would expect to be able to correctly identify larger bulges at higher redshift and smaller bulges to lower redshift. For our bulgeless sample, only 8% of these galaxies fall below $z = 0.06$. From this we conclude that the number of bulgeless galaxies we have identified may be an overestimate as, with higher resolution

images, we are likely to find bulges in the large fraction of these galaxies at $z > 0.06$.

3 X-RAY SMBH SAMPLE SELECTION

3.1 CSC-SDSS Cross-Match Catalog

In our first analysis, which we now describe, we investigated the properties of a sample of galaxies containing AGN selected via their X-ray detection. In order to achieve this purpose we utilized the Chandra Source Catalog/Sloan Digital Sky Survey (CSC-SDSS; Evans et al. 2010) cross-match catalogue¹ to select active black holes via their X-ray emission. The X-ray color (or hardness ratio), often used to identify AGN, was left unconstrained in this selection process in order to avoid filtering out some AGN candidates, as, for example, many of the brightest X-ray sources are identified as AGN candidates by the Wide-field Infrared Survey Explorer (WISE; Wright et al. 2010), regardless of their hardness ratio (Wang et al. 2004; Stern et al. 2012). In total, 8,997 galaxies in the SDSS were cross-matched to a Chandra X-ray detection. Of these, we subsequently identified 688 as having been assigned structural parameters in the catalog of S11. Finally, after applying our selection criteria of $n_g < 1.5$

¹ <http://cxc.harvard.edu/cgi-gen/cda/CSC-SDSSxmatch.html>

and $B/T < 0.1$, we were left with a sample of 26 galaxies classified as bulgeless.

3.2 Redshift Distribution and Structural Parameters

In order to gain some insight into the nature of our of X-ray selected sample of 688 galaxies with structural parameters, we examined their redshift and structural parameter distributions and compared them to the general population. The redshift distribution of the X-ray selected sample has been plotted in Figure 1, while the distributions in Sérsic index, bulge fraction and bulge Sérsic index are depicted in Figure 2. The Sérsic profile index was plotted only for galaxies better fitted with a Sérsic model, i.e. with an F-test probability $P_{pS} > 0.32$ (S11), whereas both the bulge fraction and the bulge Sérsic index were plotted only for galaxies better fitted with a bulge + disk components model, in this case with $P_{pS} \leq 0.32$. The shape of the redshift distribution was found to be similar to that of S11 (see Figure 1), with a peak at $z \sim 0.1$, indicating no obvious redshift bias in the X-ray sample. However, the distribution in Sérsic profile was found to differ, being flatter at low n_g , and possessing no prominent preferred value at $n_g = 1$, contrary to what was seen in the general population (see Figure 2). Similarly, the distribution in bulge fraction was also found to show a deficit of $(B/T)_r < 0.3$ as compared to the general population (see Figure 2). Taken together, therefore, the structural parameter distributions seemed to indicate a bias towards non-bulgeless galaxies in our X-ray selected sample.

3.3 Stellar Mass Estimates

One of the primary objectives of our work was to investigate the relationship between the stellar masses of our galaxies and their supermassive black holes. In order to obtain estimates of the stellar masses of our sample, we made use of the catalog of Mendel et al. (2012, hereafter M12). In this work, M12 estimated the stellar masses of 669,634 galaxies in the Legacy area of the SDSS DR7, with spectroscopic redshifts in the range $0.005 \leq z \leq 0.4$. Importantly for us, M12 considered only sources classified as galaxies both photometrically and spectroscopically by the SDSS, i.e. sources with `photoObj.type = 3` and `specObj.specClass = 2`. A key consequence of the nature of this selection was that it should have had the effect of filtering out most of the unobscured (type 1) AGN, i.e. those showing broad emission lines. Crucially, this implies that our final sample possessing stellar masses, obtained from the catalog of M12, both for this analysis and the analysis in Section 4, should have been composed mainly of obscured (type 2) AGN. Although, this might be viewed as a restriction, as ideally one would like to have a sample composed of both types of AGN, there are two immediate benefits to having a sample composed of type 2 AGN. The first is that this provides an opportunity to study SMBHs in type 2 AGN on a large scale. The second benefit of obtaining such a sample is that one can expect a minimal contribution from obscured AGN to the total optical light in these galaxies, and hence, a negligible effect from the AGN optical light to the estimates of their stellar masses.

The stellar masses obtained by M12 were derived via

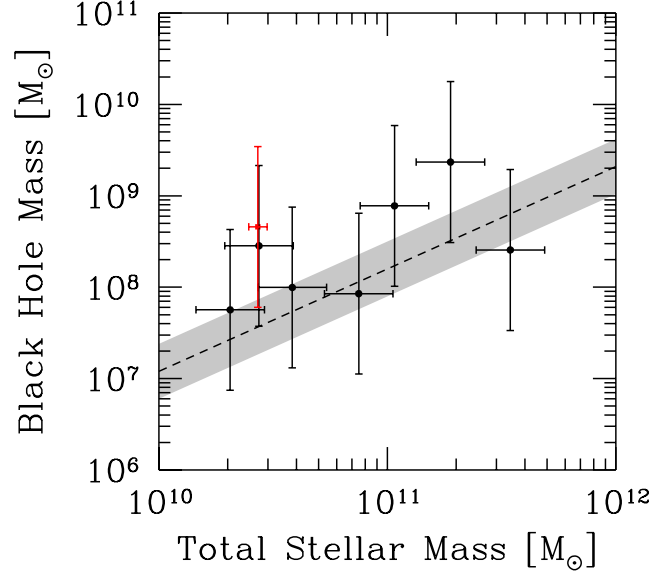


Figure 3. Total stellar mass versus black hole mass estimated from the fundamental plane of BH activity for our X-ray/radio sample (*black filled circles*). The bulgeless galaxy is shown as a *red filled square*. The horizontal error bars correspond to the 0.04 and 0.15 dex for the single- and two-component SED fits associated with the stellar mass estimates, respectively (M12), while the vertical error bars correspond to $\sigma_R = 0.88$ of the fundamental plane of BH activity (Merloni et al. 2003). For comparison, we also plot the empirical relation (*dashed line*) and the observed scatter of 0.3 dex (*grey shaded region*) of Häring & Rix (2004).

the fit of the spectral energy distribution (SED) of SDSS *ugri* photometry with the flexible stellar population synthesis code of Conroy et al. (2009). For our selected sample of bulgeless galaxies, we used the total stellar mass estimates from the Sérsic profile fitting (M12, Table 2). While for the remainder of our sample, we used the total, bulge and disk stellar mass estimates from the de Vaucouleurs bulge + exponential disk fitting (M12, Table 3). It is important to note that the fit to the total, bulge and disk photometry was carried out independently and, therefore, it is not necessarily true that $M_{*b} + M_{*d} \equiv M_{*t}$. Based on Monte Carlo simulations, the uncertainties in stellar mass are estimated to be 0.04 and 0.15 dex for the single- and two-component fits, respectively (M12). Of the 688 galaxies in our X-ray/morphology sample, we were able to match 404 galaxies with the M12 catalog and get their stellar masses.

3.4 Black Hole Mass Estimates from Fundamental Plane of BH Activity

To compute an estimate of the black hole mass for our X-ray sample, we appealed to the fundamental plane of black hole activity (Merloni et al. 2003), which correlates the X-ray and radio luminosities with the mass of the black hole.

In order to search for the level of radio emission from the detected Chandra X-ray sources in our galaxy sample, we utilized the source catalog produced by the National Radio Observatory/Very Large Array (NRAO/VLA) Sky Survey

Table 1. Stellar Mass Estimates

SDSS objid	$\log(M_t/M_\odot)$	$\log(M_b/M_\odot)$	$\log(M_d/M_\odot)$
587727229448421420	10.3488	9.5920	10.3382
588015508739195010	11.2763	11.2495	10.3101
587731513142673426	11.0313	10.8544	10.5517
587731513142673623	10.4378	9.8747	10.2581
587731513678561426	10.3119	10.2140	10.2791
587731513687670913	11.5380	11.4924	10.9015
587724199889666262	10.5839	10.4694	10.4105
587730775500128413	10.8746	11.1970	8.6308

Table 2. Structural Parameter

SDSS objid	z	n_g	$(B/T)_r$	n_b	P_{pS}
587727229448421420	0.048	0.95	0.00	5.84	0.500
588015508739195010	0.097	4.97	0.95	5.77	0.440
587731513142673426	0.045	4.18	0.65	3.62	0.210
587731513142673623	0.043	1.28	0.22	3.13	0.170
587731513678561426	0.094	3.72	0.94	3.58	0.500
587731513687670913	0.181	4.66	0.83	4.03	0.530
587724199889666262	0.041	0.68	0.28	1.76	0.020
587730775500128413	0.114	3.00	0.54	6.34	0.270

(NVSS). This radio survey was undertaken by the NRAO VLA telescope and covered the sky north of a declination of -40 degrees, at a frequency of 1.4 GHz, a resolution of 45" and a limiting peak source brightness of about 2.5 mJy/beam. Of the 404 sources that we had previously identified as having been assigned a stellar mass in the M12 catalog, we managed to find 8 that also had an NVSS radio detection, one of which we identified as bulgeless. The stellar masses of our final 8 galaxies are given in Table 1, while their morphological parameters are listed in Table 2. We note that the galaxy 587724199889666262 can also be found in the 2MASS-selected Flat Galaxy Catalog of Mitronova et al. (2004).

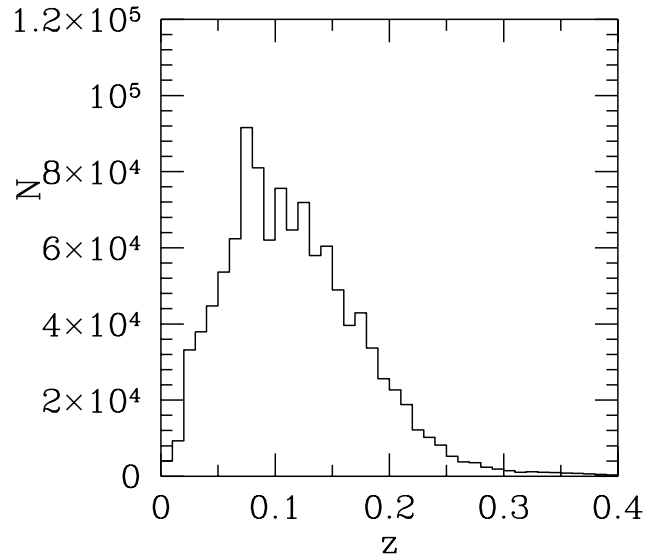
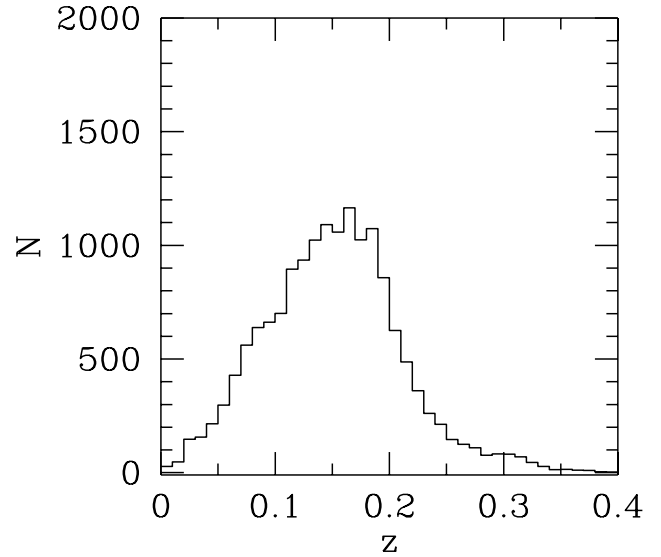
The empirical relationship relating black hole mass to the emitted compact radio and hard X-ray luminosities, spanning nine orders of magnitude in black hole mass, is formalized by the equation

$$\log L_R = (0.60_{-0.11}^{+0.11}) \log L_X + (0.78_{-0.09}^{+0.11}) \log M + 7.33_{-4.07}^{+4.05}, \quad (1)$$

where L_R is the radio luminosity at 5 GHz in erg/s, L_X is the 2-10 keV X-ray luminosity in erg/s, and M is the mass of the black hole in solar masses. The scatter around this plane is $\sigma_R = 0.88$ (Merloni et al. 2003).

The observed 1.4 GHz radio flux densities were corrected to the 5 GHz frequency by assuming a power-law emission of $S \propto \nu^{-0.7}$ at these frequencies, i.e. $S_{5\text{GHz}} = 0.41 S_{1.4\text{GHz}}$. The correction to the rest-frame flux densities was carried out by applying a multiplicative factor of $(1+z)^{0.7}$. The flux densities were also corrected for the effect of bandwidth compression by applying the multiplicative term $(1+z)^{-1}$. The mass estimates of the black holes for our final sample of 8 galaxies selected via their X-ray/radio emission are given in Table 3.

The correlation between black hole mass and total stellar mass for our sample of 8 galaxies, including the one classified as bulgeless, is shown in Figure 3. For comparison, we show in the same figure the empirical relation of Häring & Rix (2004) (dashed line) derived using dynamical

**Figure 4.** *Top:* Redshift distribution of the 15,991 WISE color selected AGN with structural parameters. *Bottom:* Redshift distribution of the SDSS DR7 galaxies in the S11 morphological catalog.**Table 3.** Estimated Black Hole Mass

SDSS objid	$\log(L_R)$	$\log(L_X)$	$\log(M/M_\odot)$
587727229448421420	40.916	38.634	8.6598
588015508739195010	40.476	38.924	9.3690
587731513142673426	41.225	38.999	8.8898
587731513142673623	39.609	37.689	8.4525
587731513678561426	42.095	38.634	7.7521
587731513687670913	42.097	39.146	8.4072
587724199889666262	40.506	37.871	7.9969
587730775500128413	43.188	39.427	7.9291

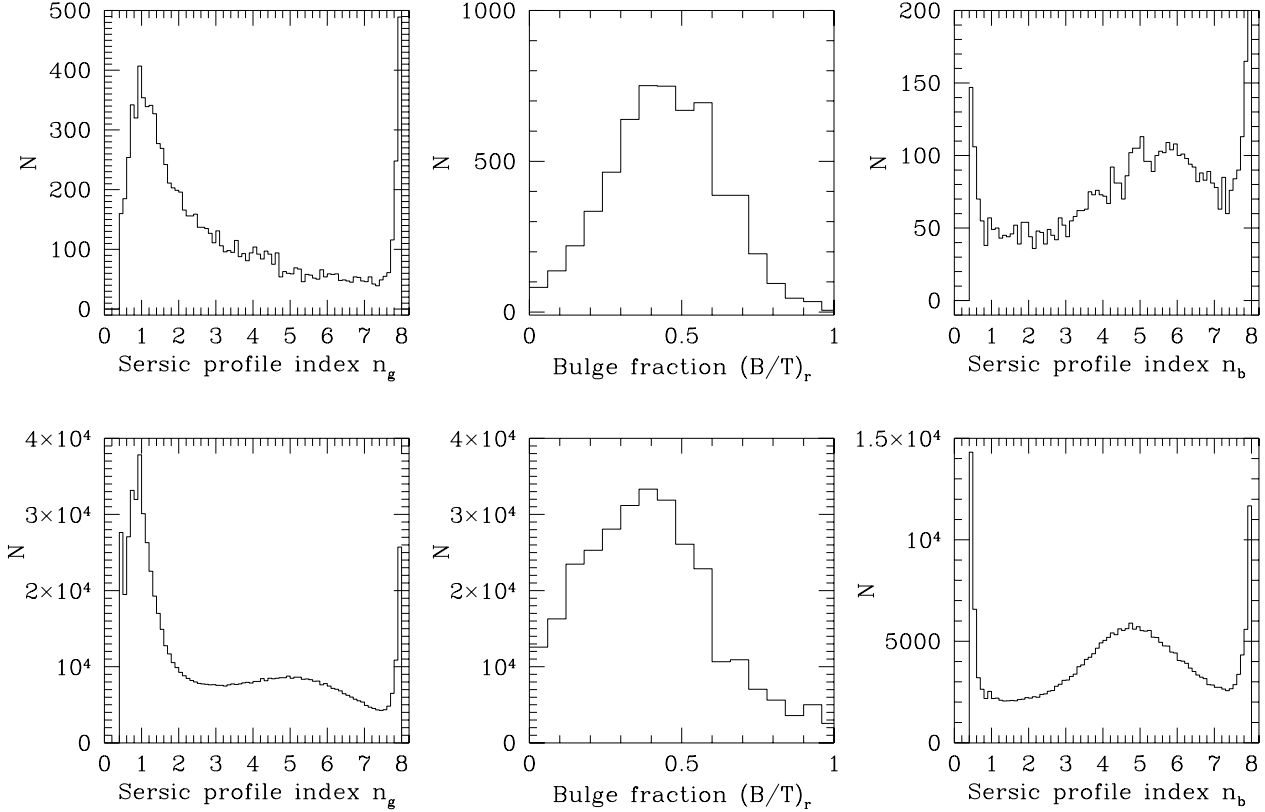


Figure 5. *Top row:* Distribution of the Sérsic profile index n_g (left), the bulge fraction $(B/T)_r$ (middle) and the bulge Sérsic index n_b (right) of the WISE color selected AGN with structural parameters. *Bottom row:* Distribution of the Sérsic profile index n_g (left), the bulge fraction $(B/T)_r$ (middle) and the bulge Sérsic index n_b (right) of the SDSS DR7 galaxies in the S11 morphological catalog.

cal and stellar masses of *bulge-dominated* systems, for which $M_{*b} \simeq M_{*t}$. In contrast, our *total stellar masses* are based either on the Sérsic profile fitting (for our bulgeless galaxy) or the de Vaucouleurs bulge + exponential disk profile fitting (for the remainder of the sample). The fact that the correlation between black hole mass and total stellar mass is consistent with the relation of Häring & Rix (2004) suggests that the true correlation might not be with the bulge mass but rather with the total stellar mass. That this is indeed the case becomes clearer in our second study, which we now detail.

4 INFRARED SMBH SAMPLE SELECTION

4.1 WISE-SDSS Cross-Match Catalog

In our second analysis, we utilized the WISE all-sky catalog to identify both unobscured (type 1) and obscured (type 2) AGN. In this regard, it is important to note that most surveys of AGN that have previously been undertaken have been biased towards observing mainly unobscured (type 1) AGN, even though theoretical models generally predict a large population of obscured (type 2) AGN, outnumbering type 1 AGN by a factor of ~ 3 (e.g. Comastri et al. 1995; Treister et al. 2004; Ballantyne et al. 2011). A key advantage to using the mid-infrared selection of AGN is that it

does not suffer from this bias, as it relies upon distinguishing the approximately power-law AGN spectrum from the black body stellar spectrum of galaxies which peaks at rest-frame $1.6\mu\text{m}$, and is thereby able to identify both unobscured (type 1) and obscured (type 2) AGN. Another advantage to working with mid-infrared data is that they allow AGN to be easily distinguished from stars and galaxies. Furthermore, an added benefit of mid-infrared selection is that it does not suffer from dust extinction and is sensitive to the highest redshift sources.

In order to obtain our infrared sample we downloaded part22 to part50 of the WISE All-Sky Catalog (covering the area covered by SDSS, i.e. $\text{dec} > -23.1899$ degrees). The WISE All-Sky Release Source Catalog contains positions and photometry at 3.4, 4.6, 12 and 22 micron for 563,921,584 point-like and resolved objects detected on the Atlas Intensity images. Photometry was performed using point source profile-fitting and multi-aperture photometry and the estimated sensitivities are 0.068, 0.098, 0.86 and 5.4 mJy (5σ) at 3.4, 4.6, 12 and 22 micron in unconfused regions on the ecliptic plane. J2000 positions and uncertainties were reconstructed using the 2MASS Point Source Catalog as astrometric reference. Astrometric accuracy is approximately 0.2 arcsec root-mean-square on each axis with respect to the 2MASS reference frame for sources with signal-to-noise ratio greater than forty.

Based on their distinctive spectral energy distribu-

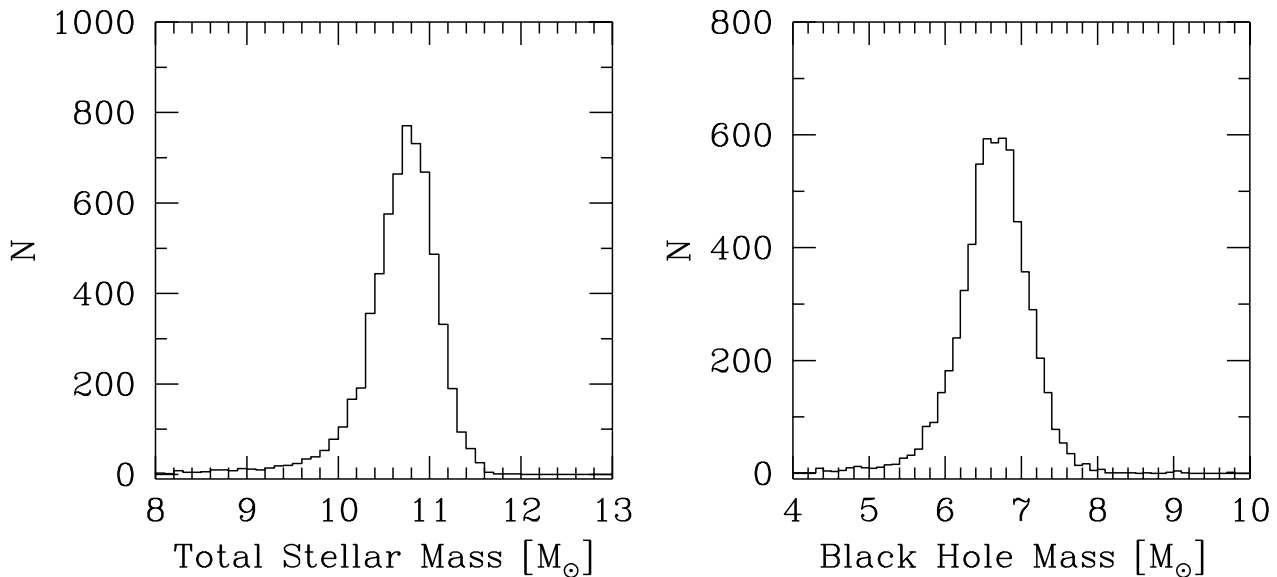


Figure 6. Distribution of the total stellar masses (*left*) and lower limits on black hole masses ($L_{bol} = L_{Edd}$, *right*) of the 6,247 WISE color selected AGN with structural parameters and stellar masses.

tion in the infrared (Wu et al. 2012; Stern et al. 2012; Assef et al. 2010), we selected AGN in the WISE all-sky catalog out to a redshift of $z \sim 3.5$ by applying the mid-infrared color criterion $W1 - W2 \geq 0.57$ (Stern et al. 2012; Wu et al. 2012). We found that $\sim 15\%$ of the WISE sources satisfied this criterion (from a total of 3.27072×10^8 sources, we were left with 51,048,962.)

Having obtained our initial sample we then used the US Virtual Astronomical Observatory (VAO) Cross-Comparison Tool to upload the WISE-selected AGN catalog and cross-matched this with the online SDSS DR 7 catalog, using a 0.5 arcsec match radius (Stern et al. 2012, positional accuracy with 2MASS). The number of cross-matched sources equaled 6,969,533, corresponding to about 2% of the initial sample. In total, 15,991 galaxies were found to have structural parameters derived by S11 and we subsequently found that 1,450 of these galaxies (or about 9%) satisfied our bulgeless selection criteria.

4.2 Redshift Distribution and Structural Parameters

The distributions of our WISE color selected AGN galaxy population have been plotted in Figures 4 and 5, as a function of their redshift, z , and structural parameters, n_g , $(B/T)_r$ and n_b , respectively. As in Figure 2 of Section 3.2, the Sérsic profile index was plotted only for galaxies with $P_{ps} > 0.32$ (S11), whereas both the bulge fraction and the bulge Sérsic index were plotted only for galaxies with $P_{ps} \leq 0.32$. Simple consideration of these distributions lead to some important new results regarding the properties of AGN and, therefore, more generally for galaxies containing SMBH.

The first, and most important of these statistical results, which can be immediately seen in the distribution of

the Sérsic index of our infrared selected sample, Figure 5 (left), is that the AGN are smoothly and significantly distributed over all values of n_g . This necessarily implies that *AGN in our sample, and therefore their associated SMBH, are present in galaxies of all morphological types.* This is a key discovery, as until now relatively few SMBH were known to exist in galaxies that did not possess a significant bulge component.

The second important statistical result, is that the morphological distributions of the AGN sample and the general population of galaxies have a very similar form. This can be clearly seen by comparing the Sérsic distribution of the infrared selected AGN, Figure 5 (top left), with that of the parent population Figure 5 (bottom left). Alternatively, comparing Figure 5 (top middle and right) with Figure 5 (bottom middle and right), similarly reveals that in the case when the galaxies have been fitted with a bulge + disk component model, the galaxies with a SMBH again follow a very similar distribution of bulge fraction and bulge Sérsic index to the general population of galaxies. To quantify this statement, we used the Kolmogorov-Smirnov (K-S) test to measure the probability that our first dataset is drawn from the same parent population as our second dataset (the two-sample K-S test). The probability is a scalar between 0 and 1 giving the significance level of the K-S statistic. Small values of the K-S probability show that the cumulative distribution function of the first dataset is significantly different from the second dataset. The results of the K-S test reinforce our qualitative comparison: after normalizing each distribution to the total number count and using the same bin size as depicted in Figure 5, we compute K-S probabilities and maximum deviations between datasets of (0.99,1.0,1.0) and (0.02,0.004,0.01) for the distribution of $(n_g, (B/T)_r, n_b)$, respectively, indicating a very high probability that these three distributions are the same.

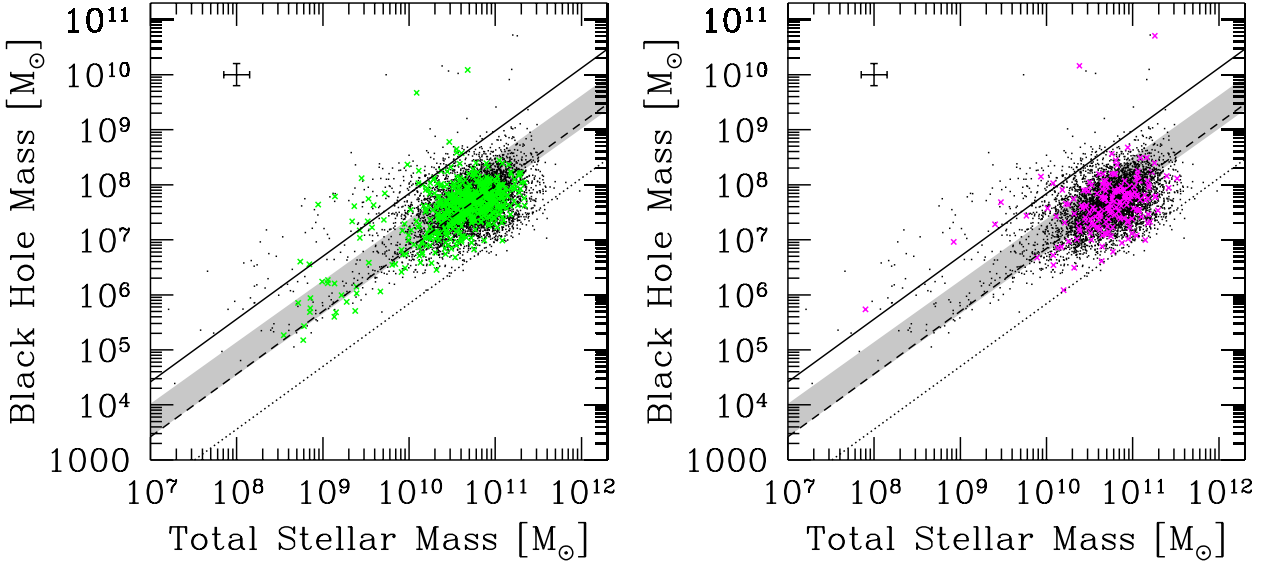


Figure 7. *Left:* Total stellar mass versus black hole mass obtained using the bolometric luminosity for our infrared sample of 5,717 galaxies not classified as bulgeless (*black dots*) and for the 530 bulgeless galaxies (*green crosses*). The data points and bisector linear regression fit to the data (*dashed line*) are plotted for $L_{bol}/L_{Edd} = 0.1$. Also shown are the fit for $L_{bol}/L_{Edd} = 1.0$ (*dotted line*) and for $L_{bol}/L_{Edd} = 0.01$ (*solid line*). For comparison, we also plot the observed scatter of 0.3 dex of the empirical relation of Häring & Rix (2004) (*grey shaded region*). *Right:* Same as left figure, showing in addition the galaxies with $3.9 < n_b < 4.1$ highlighted as *magenta crosses*.

Hence, from these comparisons we learn that not only are the SMBH in our infrared selected sample distributed over all morphological galaxy types, but that the form of their morphological distribution is very similar to that of the general population of galaxies, over the same redshift range, i.e. $0.05 < z < 0.25$. Moreover, this similarity property is essentially robust with respect to the form of morphological fitting that is used. An immediate consequence of this approximate scaling relation between the distributions of the AGN and the general population, is that it implies that *the fraction of galaxies that contain a SMBH is approximately the same for each morphological type*. Alternatively, one may say that the fraction of a particular type of galaxy is the same in both the AGN and general populations. In particular, the fraction of bulgeless galaxies that host a SMBH is the same as the fraction of bulgeless galaxies in the general population, which is $\sim 9\%$ in the redshift range considered.

An important set of questions concern the extent to which our statistical sample may be assumed to be representative of the entire population of AGN galaxies and the general population of galaxies with SMBH in the Universe. In the strictest sense the above results apply only to our sample of infrared selected AGN. However, if our sample is representative, which we reasonably expect it is, then it is also reasonable to extrapolate the above results to the general population of galaxies containing AGN. Furthermore, as the results of this analysis suggest that AGN do not appear to significantly distinguish between different galaxy morphologies, at least at the level we can detect, it seems difficult to construct an argument to support the idea that the more general population of galaxies with a SMBH (i.e. active and

inactive galactic nuclei) does. Moreover, if it is the case that the above statistical results can be extrapolated to the general population of galaxies containing a SMBH, they have an important corollary. Since it follows that if the current widely held opinion (and its supporting evidence) that most, if not all, massive ellipticals and galaxies with bulges contain a SMBH is valid, then essentially the same must apply to all the others, i.e. *most galaxies do contain a SMBH*.

In comparing the redshift distribution of the WISE color selected AGN with structural parameters with that of the SDSS DR7 galaxies in the S11 morphological catalog (see Figure 4), we noted a sharper fall-off toward lower redshifts together with an associated shift in the peak of the distribution from about 0.1 to 0.2. This marked difference between the two distributions originates from the removal of apparently non-AGN galaxies from the sample at low redshifts by the WISE cross-match selection process. One possible reason for this apparent reduction of galaxies with AGN toward low redshifts could of course be the absence or paucity of SMBH in more recently formed galaxies. However, if this were the case, then as one would expect newly formed galaxies to be biased toward particular morphology types, one should similarly expect to see a difference between the distribution of AGN in these morphology types with respect to the general population, which as we have seen is not obviously apparent. Hence, we are led to interpret the apparent depletion of AGN toward low redshifts as being more likely primarily due to the decrease in AGN activity toward low redshifts. Or, in other words, it would seem that the difference between the two redshift distributions should not be taken to imply that there exist fewer

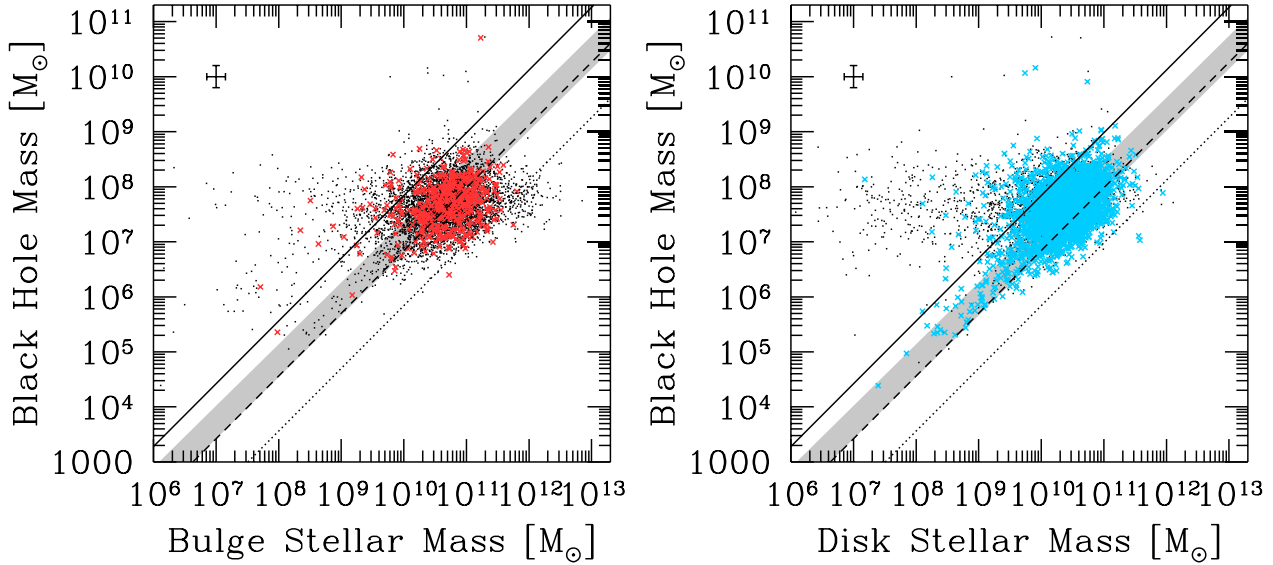


Figure 8. Bulge (*left*) and disk stellar mass (*right*) versus black hole mass obtained using the bolometric luminosity for our infrared sample of 5,717 galaxies not classified as bulgeless (*black dots*). The bulge-dominated galaxies only ($(B/T)_r \geq 0.5$) are highlighted as *red crosses* in the *left figure* and the disk-dominated galaxies only ($(B/T)_r < 0.5$) are highlighted as *blue crosses* in the *right figure*. As in Figure 7, the data points and bisector linear regression fit to the data (*dashed line*) are plotted for $L_{bol}/L_{Edd} = 0.1$. Also shown are the fit for $L_{bol}/L_{Edd} = 1.0$ (*dotted line*) and for $L_{bol}/L_{Edd} = 0.01$ (*solid line*). For comparison, we also plot the observed scatter of 0.3 dex of the empirical relation of Häring & Rix (2004) (*grey shaded region*).

supermassive black holes in galaxies at lower redshifts, but merely that black holes become on average less active. This property, which is well known (e.g. Fan 2006), can be seen for instance in the photometric redshift distribution of the SDSS quasars and their WISE counterparts, as depicted in Figure 2 of Wu et al. (2012). Although here, by contrast, we stress that we are witnessing this effect in both the type 1 and type 2 AGN galaxy populations.

4.3 Stellar Mass Estimates

Finally, we turn our attention to the relationship between the stellar and black hole masses for our infrared selected sample of galaxies with AGN. Following the description in Section 3.3 above, we obtained the stellar masses of 6,247 galaxies in this sample from Mendel et al. (2012). As described in Section 3.3, the selection of sources with stellar masses from Mendel et al. (2012) implied that we preferentially selected obscured (type 2) AGN. In a similar fashion to our X-ray/radio sample, we used the Sérsic profile total stellar mass estimates for our 530 bulgeless galaxies and the de Vaucouleurs + exponential profile total, bulge and disk stellar mass estimates for the remainder of our sample. The distribution of total stellar masses is shown in Figure 6 (left). For clarity, the sizes of the statistical samples used in our analysis are summarized in Table 4.

Table 4. Sizes of Statistical Samples

Sample	No. Galaxies	No. Bulgeless
S11 catalogue:	1,123,718	155,040
S11 + $0.05 < z < 0.25$:	946,299	110,913
WISE catalogue:	3.27072×10^8	N/A
WISE + $W1 - W2 \geq 0.57^a$:	51,048,962	N/A
WISEcol + SDSS:	6,969,533	N/A
WISEcol + SDSS + S11:	15,991	1,450
WISEcol + SDSS + S11 + M12:	6,247	530
CSC-SDSS catalogue:	8,997	N/A
CSC-SDSS + NVSS:	34	N/A
CSC-SDSS + S11:	688	26
CSC-SDSS + NVSS + S11:	10	1
CSC-SDSS + NVSS + S11 + M12:	8	1

^a hereafter WISEcol.

4.4 Black Hole Mass Estimates from the Bolometric Luminosity

Black hole masses were estimated using the bolometric luminosity of the galaxies. Bolometric luminosities (taken to be the 100 micron to 10 keV integrated luminosity Richards et al. 2006) are typically obtained using corrections to the mid-infrared bands where the AGN emission dominates. We used the 12 (W3) and 22 micron (W4) k-corrected flux densities from WISE to compute the bolometric luminosities of our WISE color-selected AGN and applied the bolometric corrections $L_{bol} \simeq 8 \times L_{12\mu m}$ (W3) and $L_{bol} \simeq 10 \times L_{22\mu m}$ (W4) from Richards et al. (2006), which are not strongly dependent on AGN luminosity (see their Figure 12). Given the bolometric luminosity, making the assumption that accretion is at the Eddington limit

yields a lower limit on the black hole mass. However, given that the growth rates of AGN can span several orders of magnitude, from super-Eddington accretion to $10^{-3}L_{Edd}$ (Simmons et al. 2013; Steinhardt & Elvis 2010), we computed black hole masses assuming the following three cases: $L_{bol} = L_{Edd}$, $L_{bol} = 0.1L_{Edd}$, and $L_{bol} = 0.01L_{Edd}$. The histogram of BH masses ($L_{bol} = L_{Edd}$) is shown in Figure 6 (right). The black hole masses range from $10^5 M_{\odot}$ to $10^8 M_{\odot}$ with a peak near $\sim 4 \times 10^6$. These numbers are consistent with those measured in the sample of Simmons et al. (2013) ($10^5 M_{\odot}$ to $10^6 M_{\odot}$) given our larger sample size. However, they are statistically lower than the masses measured from our X-ray/radio sample.

Using the stellar masses of Mendel et al. (2012) and the black hole masses estimated from the bolometric luminosity of the galaxies, we present the correlation between black hole mass and total stellar mass for our sample of 6,247 galaxies, including the 530 classified as bulgeless in Figure 7 (left). Here, we only show the results based on the 22 micron luminosities, although the results based on the 12 micron luminosities are very similar.

The first thing to note is that the results of using our new method of selecting AGN based on their infrared colors clearly confirm the strong correlation between the total stellar mass of galaxies and the mass of their SMBHs. However importantly, whereas previous studies were limited to primarily bulge-dominated systems, our study confirms this relationship to *all morphological types, in particular, to bulgeless galaxies* (Figure 7 left, green crosses). Additionally, we emphasize that this study is by far the largest sample to date.

In this figure, the total stellar mass estimates for the bulgeless galaxies are from the Sérsic profile fitting (Figure 7 left, green crosses) whereas the rest are from the de Vaucouleurs bulge + exponential disk fitting (Figure 7 left, black dots). For reference to previous work done for classical bulges, we show in the same figure the sample of galaxies with bulge Sérsic index $3.9 < n_b < 4.1$ (Figure 7 right, magenta crosses). It may be noted that the location of these galaxies in the diagram is almost indistinguishable from the bulgeless galaxies.

A bisector linear regression fit to the data leads to the relation:

$$\log \left(\frac{M_{bh}}{M_{\odot}} \right) = \alpha + \beta \log \left(\frac{M_{\star t}}{10^{11} M_{\odot}} \right), \quad (2)$$

where $\alpha = 7.98 \pm 0.20$ and $\beta = 1.14 \pm 0.10$ for $L_{bol}/L_{Edd} = 0.1$. This relation is plotted in Figure 7 with a dashed line. The relations obtained using $L_{bol}/L_{Edd} = 1.0$ and $L_{bol}/L_{Edd} = 0.01$ are also shown for comparison with a dotted and solid line, respectively.

For comparison, we have also shown in the same figure the empirical relation of Häring & Rix (2004) (where $\alpha = 8.20 \pm 0.10$, $\beta = 1.12 \pm 0.06$, and scatter of 0.3 dex, grey shaded region). Although the slopes of the two fits are essentially the same, the agreement on the intercept depends on the value of L_{bol}/L_{Edd} . Assuming that previous studies such as that of Häring & Rix (2004) based on local dynamical mass estimates are correct, then our results appear to be most consistent with the black hole masses derived using $L_{bol}/L_{Edd} = 0.1$. In fact, we expect this assumption to be the main source of uncertainty in our analysis, as the errors

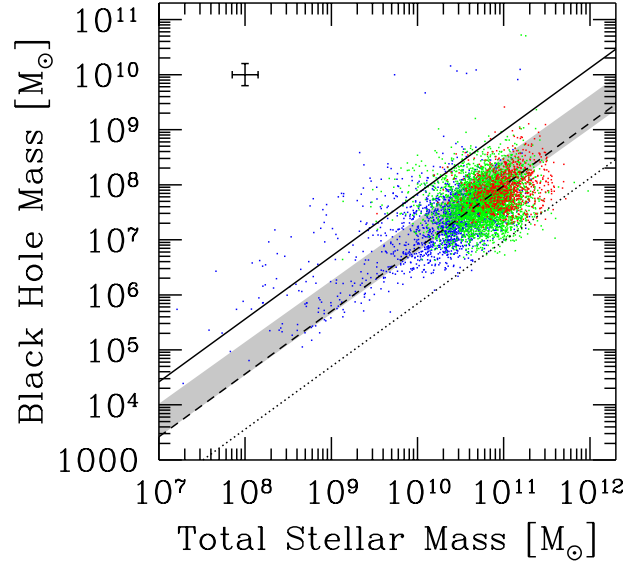


Figure 9. Same as Figure 7, with galaxies divided in three redshift bins: $z < 0.1$ (blue), $0.1 \leq z < 0.2$ (green), and $z \geq 0.2$ (red).

that arise from estimating the total stellar masses are on average ~ 0.15 dex and those from estimating the bolometric luminosity are on average ~ 0.20 dex, and hence cannot account for such a shift. Indeed, in this regard, Simmons et al. (2013) point out that accretion may take place at well below the Eddington limit and find that, at least for two sources in their sample, $L_{bol}/L_{Edd} = 0.05$ and 0.08 . Hence, if a growth rate of order $L_{bol}/L_{Edd} = 0.1$ is typical of the sample, it implies that our black hole and total stellar mass relation is consistent with the empirical relation of Häring & Rix (2004).

In Figure 8, we have plotted the results which essentially represent the galaxies in our sample with a significant bulge component, specifically those that do not satisfy the bulgeless selection criteria $n_g < 1.5$ and $(B/T)_r < 0.1$. In Figure 8 (left) we consider the bulge stellar mass only, while in Figure 8 (right) we consider the disk stellar mass only. In both figures scatter is significantly increased with respect to Figure 7, which uses the total stellar mass. This indicates that the *true correlation is between the black hole mass and the total stellar mass*. This is confirmed when we consider the bulge-dominated galaxies only ($(B/T)_r \geq 0.5$) in Figure 8 (left, red crosses), and the disk-dominated galaxies only ($(B/T)_r < 0.5$) (right, blue crosses), and note that these exhibit significantly tighter correlations. Therefore, we conclude that the previous assumption that the black hole mass was correlated with the bulge mass was only approximately correct, since the true relation is in fact with the total stellar mass of the galaxy. However, the approximate bulge mass correlation therefore becomes increasingly accurate as the bulge mass dominates the total mass of the galaxy.

In Figure 9, we also provide a plot of the data sorted into three redshift bins: $z < 0.1$ (blue open circles), $0.1 \leq z < 0.2$ (green open circles), and $z \geq 0.2$ (red open circles). Com-

paring data at low redshift, it is entirely consistent with what is found based on local dynamical mass estimates. In this figure, there appears to be a deficit of low masses at high redshift. This redshift dependence is very likely due to the bias introduced by the limiting magnitudes of both the SDSS and WISE all-sky survey and not to any evolutionary effect. For instance, the minimum logarithm of the BH mass based on the flux limit of WISE at 22 micron of 5.4 mJy (5σ) and using $L_{bol} = 0.1 L_{Edd}$ is (5.0,7.0,7.7,8.0) at $z=(0.01,0.1,0.2,0.3)$, respectively.

5 SUMMARY

By using the quantitative morphological analysis of 1.12 million galaxies in the SDSS DR7 (S11), we have presented the first systematic survey of SMBHs in galaxies of all morphological types, i.e. including bulgeless galaxies. Two different methods were used to identify the presence of black holes via their activity, the first being their X-ray/radio emission and the second their mid-infrared colors. These two studies are complementary in that while our first analysis of the X-ray selected sample is biased towards selecting unobscured AGN and provides a well-tested and robust estimate of black hole mass but with a small statistic, our second analysis of the infrared selected sample includes both unobscured (type 1) and obscured (type 2) AGN and provides estimates on the black hole mass but with a large statistic.

Our first analysis identified 688 unobscured active galaxies with known structural parameters. When the Sérsic profile index n_g and bulge fraction $(B/T)_r$ of these galaxies were examined, we were able to identify 26 of these galaxies hosting a SMBH as bulgeless. We were able to obtain estimates for both the stellar and black hole masses for 8 of these 688 galaxies and investigate their relationship. The results of this first analysis confirm the correlation between black hole and total stellar mass for these 8 galaxies and includes one galaxy classified as bulgeless.

Our second analysis identified 15,991 mostly obscured active galaxies with known structural parameters. When the Sérsic profile index and bulge fraction of this sample were examined, we were able to identify 1,450 bulgeless galaxies containing AGN. Moreover, when analyzing the full range of structural parameters, we found that these active galaxies followed a very similar morphological distribution to the general population of galaxies in the same redshift range. In particular, the fraction of bulgeless galaxies, $\sim 9\%$, was found to be the same as in the general population. For this larger sample, we were also able to obtain estimates of the total stellar and black hole masses for 6,247 galaxies and investigate their relationship. Importantly, whereas previous studies were limited to primarily bulge-dominated systems, our study confirms this relationship to all morphological types, in particular, to 530 bulgeless galaxies. Furthermore, we were able to investigate the same relationship using the independently estimated bulge and disk stellar masses. Our results indicated that the true correlation is between the black hole mass and the total stellar mass and hence we concluded that the previous assumption that the black hole mass is correlated with the bulge mass was only approximately correct. If extrapolated, the combination of these results appear to indicate that SMBHs are generic to galaxies

regardless of the details of stellar galaxy evolution, dynamics and merger history of galaxies. As it is only possible to estimate dynamical masses locally, the future of studying SMBHs in galaxies at all redshifts lies in a method such as the one presented in this work.

6 FUTURE WORK

An obvious extension of our analysis, to be presented in a future paper, will be to include unobscured AGNs. For these galaxies, where the nuclear emission is clearly visible, fitting an additional component to the two-dimensional light profile will be necessary, as the fitting models used in S11 would underestimate the bulgeless fraction of the AGN sample by overestimating the Sérsic index of the host component.

REFERENCES

- Abazajian, K. et al., 2009, ApJS, 182, 543
 Assef, R.J. et al., 2010, ApJ, 713, 970
 Ballantyne D.R., Draper A.R., Madsen K.K., Rigby J.R., Treister E., 2011, ApJ, 736, 56
 Comastri A., Setti G., Zamorani G., Hasinger G., 1995, A&A 296, 1
 Conroy et al. 2009, ApJ, 699, 486
 Evans, I.N. et al., 2010, ApJS, 189, 37
 Fan, X., 2006, NewAR, 50, 665
 Ferrarese L., Merritt D., 2000, AJ, 539, L9
 Gebhardt et al. 2000, AJ, 539, 13
 Greene et al. 2010, ApJ, 721, 26
 Häring, N. Rix,H.-W., 2004, ApJ, 604, L89
 Hopkins P.F., Hernquist L., Cox T.J., Keres D., 2008, ApJS, 175, 356
 Jiang, Y.-F., Greene, J.E., Ho, L.C., Xiao, T., Barth, A.J., 2011, ApJ, 742, 68
 Kelvin, Lee, 2013, Ph.D. Thesis
 Kormendy J., Drory N., Bender R., Cornell M.E., 2010, ApJ, 723, 54
 Kormendy & Richstone 1995, ARAA, 33, 581
 Magorrian J. et al., 1998, AJ, 15, 2285
 Marleau, F.R., Simard, L., 1998, ApJ, 507, 585
 Mendel J.T., Palmer M., Simard L., Ellison S.L., Patton D.R., 2012, in preparation
 Merloni A., Heinz, S., di Matteo, T., 2003, MNRAS, 345, 1057
 Mitronova, S.N., Karachentsev, I.D., Karachentseva, V.E., Jarrett, T.H., Kudrya, Yu.N., 2004, BSAO, 57, 5
 Okamoto 2012, [arXiv:1206.5507](https://arxiv.org/abs/1206.5507)
 Reines et al. 2011, Nature, 470, 66
 Richards G.T. et al., 2006, ApJS, 166, 470
 Sanders D.B., Soifer B.T., Elias J.H., Madore B.F., Matthews K., Neugebauer G., Scoville N.Z., 188, ApJ, 325, 74
 Simard L., Mendel J.T., Patton D.R., Ellison S.L., McConnachie A.W., 2011, ApJS, 196, 11
 Simard L., Willmer C.M.A., Vogt N.P., et al., 2002, ApJS, 142, 1
 Simmons, B.D., Lintott, C., Schawinski, K., Moran, E.C., Han, A., Kaviraj, S., Masters, K.L., Urry, C.M., Willett,

- K.W., Bamford, S.P., Nichol, R.C., 2013, MNRAS, 429, 2199
Steinhardt, C.L., Elvis, M., 2010, MNRAS, 402, 2637
Stern D. et al., 2012, [arXiv:1205.0811](#)
Treister E. et al., 2004, ApJ, 616, 123
Volonteri, M., 2012, [arXiv:1209.1195v1](#)
Wang J.X. et al., 2004, AJ, 127, 213
White S.D.M., Frenk C.S., 1991, ApJ, 379, 52
White S.D.M., Rees M.J., 1978, MNRAS, 183, 341
Wright, E.L. et al., 2010, AJ, 140, 1868
Wu X.-B., Hao G., Jia Z., Zhang Y., Peng N., 2012, [arXiv:1204.6197](#)
York, D.G. et al., 2000, AJ, 120, 1579